Noname manuscript No.
(will be inserted by the editor)

Intrinsic Nonlinearity and Method of Disturbed Observations in Inverse Problems of Celestial Mechanics

Victor A. AVDYUSHEV

the date of receipt and acceptance should be inserted later

Abstract Orbit determination from a small sample of observations over a very short observed orbital arc is a strongly nonlinear inverse problem. Meanwhile, in problems like that an evaluation of orbital uncertainty due to random observation errors is greatly complicated since linear estimations conventionally used are no longer acceptable for describing the uncertainty even as a rough approximation. Nevertheless, if an inverse problem is weakly intrinsically nonlinear then one can resort to the so-called method of disturbed observations (aka observational Monte Carlo).

Previously, we showed that the weaker the intrinsic nonlinearity, the more efficient the method, i.e. the more accurate it enables one to stochastically simulate the orbital uncertainty, while it is strictly exact only when the problem is intrinsically linear. However, as we ascertained experimentally, its efficiency was found to be higher than that of other stochastic methods widely applied in practice.

In the present paper we investigate the intrinsic nonlinearity in complicated inverse problems of celestial mechanics when orbits are determined from little informative samples of observations, which typically occurs for recently discovered asteroids. To inquire into the question we introduce an index of intrinsic nonlinearity. In asteroid problems it evinces that the intrinsic nonlinearity can be strong enough to appreciably affect probabilistic estimates, especially at the very short observed orbital arcs that the asteroids travel on for about a hundredth of their orbital periods and less.

As is known from regression analysis, the source of intrinsic nonlinearity is the nonflatness of the estimation subspace specified by a dynamical model in the observation space. Our numerical results evidence that when determining asteroid orbits it is actually very slight. However, in the parametric space the effect of intrinsic nonlinearity is exaggerated mainly by the ill-conditioning of the inverse problem.

Even so, as for the method of disturbed observations, we conclude that it practically should be still entirely acceptable to adequately describe the orbital uncertainty since, from a geometrical point of view, the efficiency of the method directly depends only on the nonflatness of the estimation subspace and it gets higher as the nonflatness decreases.

Keywords orbital motion · inverse problem · intrinsic nonlinearity

Celestial Mechanics and Astrometry Department, Applied Mathematics and Mechanics Institute, Tomsk, Russia, 634050, E-mail: sch@niipmm.tsu.ru

1 Introduction

Observations of any celestial body are littered with various errors uncorrectable owing to their randomness. When determining the orbit of a space object from observations like those, the observation errors are inevitably transmitted to the determined parameters of an adopted orbital model. Thus orbit determination is always associated with orbital uncertainty caused by random errors of observations.

Meanwhile, numerical evaluation of the uncertainty in orbital parameters is generally implemented using stochastic simulation (Chernitsov et al., 1998; Virtanen et al., 2001; Bordovitsyna et al., 2001; Williams et al., 2005; Muinonen et al., 2006; Avdyushev and Banschikova, 2007; Milani and Gronchi, 2009; Desmars et al., 2009; Avdyushev, 2009; Emel'yanov, 2010; Avdyushev, 2011). In common practice, very often one resorts to linear evaluation: from observations of a celestial body one determines its orbit by some technique of regression analysis, as a rule, that of least squares (LS); one estimates the covariance matrix of orbital parameters; and by a Monte Carlo method one simulates a cloud of virtual dynamic states of the celestial body in the parametric space. The density of this uncertainty cloud corresponds to the probability density of a multidimensional normal distribution.

This approach is rigorously valid only for linear models, i.e. when the connection between observations and parameters is linear. Orbital models are nonlinear. However, if the nonlinearity is weak over the set of virtual dynamic states then the approach in terms of linear estimations is quite acceptable as well.

If the nonlinearity is strong then the scatter of virtual dynamic states will not correspond to a normal distribution. In this case for simulating the uncertainty cloud one can use the so-called method of disturbed observations (Press et al., 1987; Avdyushev, 2009, 2010, 2011) (aka observational Monte Carlo)[1]. It consists in repeatedly determining orbital parameters from disturbed observations obtained by adding to the original ones a normal noise with zero mean and an observational error variance. This technique is widely used in practice, although its applicability is also restricted since it is valid only if the estimation subspace specified by an orbital model in the observation space is flat (Avdyushev, 2011).

In any linear problem the estimation subspace is flat. It means that there exists such a rectangular coordinate system that can span the estimation subspace in the observation space. However, the same flat subspace can be spanned by a curvilinear coordinate system, and if one takes the curvilinear coordinates as model parameters then the problem obviously gets nonlinear though it stays flat. Thus any flat problem can be both linear and nonlinear. If it is nonlinear then one can reduce it to a linear problem by an appropriate (nonlinear) transformation of parameters. In this case the problem is said to be intrinsically linear (or nonintrinsically nonlinear) (Draper and Smith, 1981).

In inverse problems of celestial mechanics the estimation subspace is not flat and it has a curvature called for convenience the normal one that is directly related to the geometry of the estimation subspace and that does not depend on a selection of determined model parameters. Consequently, if an inverse problem is not flat then it cannot be reduced to a linear one by reparametrization. Nonlinear problems like that are called intrinsically nonlinear (Draper and Smith, 1981).

In the present paper we put and try to answer the question: if the total nonlinearity is very strong (e.g. when an orbit is determined very unreliably because of a scant sample of

[1] Certainly, there exist other nonlinear methods. See e.g. in (Virtanen et al., 2001; Muinonen et al., 2006; Milani and Gronchi, 2009; Desmars et al., 2009; Emel'yanov, 2010). However, their theories bear no relation to the intrinsic nonlinearity we discuss in the paper. Those methods rather aim at solving the problem of strong so-called parameter-effect nonlinearity (Bates and Watts, 1988) than that of strong intrinsic nonlinearity.

observations) how strong can the normal nonlinearity be in the inverse problems of celestial mechanics to appreciably influence on the distribution of virtual dynamic states? To inquire into the question we introduce an index of intrinsic nonlinearity. Formerly, in (Avdyushev, 2011) another index was proposed though it enables one only to evaluate the normal curvature of the estimation subspace but tells nothing about how substantial its influence on virtual dynamic states can be.

We employ the index for studying the intrinsic nonlinearity in asteroid inverse problems, where stochastic simulation of orbital uncertainty is of very great importance (e.g. for estimating the probability of asteroid impacts with the Earth). We also assess the local nonflatness of the estimation subspace. It directly relates to the normal curvature and defines how considerable the estimation subspace differs from a flat one around the LS-estimation (obtained from observations) within a domain of observational uncertainty. The local nonflatness is interesting in that its smallness actually affords practical ground for the method of disturbed observations while, according to its geometry, the method is theoretically grounded only in the strictly flat case (Avdyushev, 2011).

2 Normal Curvature of Estimation Subspace

The problem of intrinsic nonlinearity is well-known in mathematical statistics (Beale, 1960; Draper and Smith, 1981; Bates and Watts, 1988) while it is quite unexplored in celestial mechanics. Furthermore, after our thorough examination of papers on nonlinearity (Avdyushev, 2011) we came to the conclusion that in celestial mechanics we were the first who highlighted this problem and indicated possible hardships caused by the intrinsic nonlinearity while systematically we did not yet investigate the correlation between it and conditions of inverse problems, especially with small samples of observations.

In (Avdyushev, 2011) we introduced an index of intrinsic nonlinearity as an angle between the direction from the LS-estimation point towards a given point of the estimation subspace and a flat subspace tangent to the estimation one at the LS-estimation point in the observation space. The geometric sense of the index is simple to realize in a problem with three observations ($N = 3$) and two parameters ($K = 2$). Its geometry is shown in Fig. 1. Here $\mathbf{p}^O$ is the point of observations in the 3-dimensional observation space; $\bar{\mathbf{p}}$ and $\hat{\mathbf{p}}$ on the estimation surface $\boldsymbol{\rho}$ are the points specified by a nonlinear model $\mathbf{p}^C = \mathbf{p}^C(\mathbf{q})$ with the exact parameter values $\bar{\mathbf{q}}$ and their LS-estimates $\hat{\mathbf{q}}$ respectively, the estimation surface $\boldsymbol{\rho}$ being the locus of all possible points $\mathbf{p}^C$; $\delta\mathbf{p}^O$ is the observation error vector; S is the value of the least-squares objective function, the squared distance from the point of observations $\mathbf{p}^O$ to any point of the estimation surface $\boldsymbol{\rho}$, it reaching the least value $\hat{S}^{1/2}$ for the point $\hat{\mathbf{p}}$ which is the orthogonal projection of $\mathbf{p}^O$ onto $\boldsymbol{\rho}$.

So, as we see, the angle φ can stand as an index of intrinsic nonlinearity (or local nonflatness). It is determined from the formula (Avdyushev, 2011)

$$\sin\varphi = \frac{(\mathbf{p}^O - \hat{\mathbf{p}}) \cdot (\mathbf{p}^C - \hat{\mathbf{p}})}{\|\mathbf{p}^O - \hat{\mathbf{p}}\| \, \|\mathbf{p}^C - \hat{\mathbf{p}}\|}. \tag{1}$$

To evaluate how strong the intrinsic nonlinearity influences on forming a cloud of virtual dynamic states by the method of disturbed observations, one needs to calculate the angle φ for every state and then to analyse the distribution of its values. Obviously, the major part of them must be near zero. While very large angle values are to be appreciably fewer, they are just the ones that reveal strong nonlinearity: the larger these values, the stronger the nonlinearity.

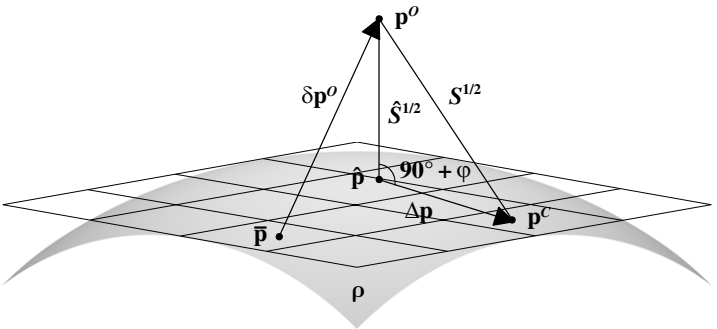

Fig. 1 Geometrical interpretation of a nonlinear LS-problem for $N = 3$ and $K = 2$. Here $\mathbf{p}^O$ is the point of observations; $\bar{\mathbf{p}}$, $\hat{\mathbf{p}}$ and $\mathbf{p}^C$ on the estimation surface $\boldsymbol{\rho}$ (grey) are the point of the exact observations, its LS-estimation and an arbitrary point respectively; the grid shows a tangent plane to the estimation surface at the estimation point $\hat{\mathbf{p}}$; $\delta\mathbf{p}^O$ is the observation error vector; $\Delta\mathbf{p}$ is the deviation of the arbitrary point $\mathbf{p}^C$ from the estimation $\hat{\mathbf{p}}$; φ is the angular deviation of the vector $\Delta\mathbf{p}$ from the tangent plane; S is the squared distance ($\hat{S}$ is the least one) from the point of observations $\mathbf{p}^O$ to the estimation surface

The main inconvenience in using the angular index consists in that an ample quantity of angle values is required for evaluating the intrinsic nonlinearity. It would be more convenient to have a different index whose single value (or maybe several values) could characterize the intrinsic nonlinearity. The curvature of the estimation subspace can be taken as an index like that. It is directly related to the curvatures of the coordinate curves

$$\mathbf{p}^i(\zeta) = \mathbf{p}^C(\hat{q}_1, \ldots, \hat{q}_{i-1}, \hat{q}_i + \zeta, \hat{q}_{i+1}, \ldots, \hat{q}_K) \quad (i = 1, \ldots, K), \tag{2}$$

where ζ is a free parameter of the i-th curve. Hereinafter $\dim \mathbf{q} = K$ and $\dim \mathbf{p} = N$. Thus, to evaluate the intrinsic nonlinearity it is necessary to calculate the normal curvatures of all the coordinate curves, and the maximum of these will just stand as that very index of intrinsic nonlinearity.

The normal curvature of every coordinate curve can be obtained as follow. First, we evaluate the variations along the coordinate curves

$$\Delta\mathbf{p}^i = \mathbf{p}^i(\Delta\zeta_i) - \hat{\mathbf{p}} \quad (i = 1, \ldots, K), \tag{3}$$

where $\Delta\zeta_i$ is a small parameter variation. Then, using the matrix of partial derivatives $\mathbf{p}'_\mathbf{q} = \partial\mathbf{p}^C/\partial\mathbf{q}$ for $\hat{\mathbf{q}}$, we compose the idempotent matrix

$$\mathbf{\Pi} = \mathbf{p}'_\mathbf{q}((\mathbf{p}'_\mathbf{q})^T\mathbf{p}'_\mathbf{q})^{-1}(\mathbf{p}'_\mathbf{q})^T \tag{4}$$

orthogonally projecting any point of the observation space onto the tangent subspace whose basis is specified by the columns of the matrix $\mathbf{p}'_\mathbf{q}$. Applying the matrix-projector to the vectors $\Delta\mathbf{p}^i$, we obtain their projections $\mathbf{\Pi}\Delta\mathbf{p}^i$ ($i = 1, \ldots, K$).

Further, for every coordinate curve we calculate the angle φ (Fig. 1):

$$\cos\varphi^i = \frac{\Delta\mathbf{p}^i \cdot \mathbf{\Pi}\Delta\mathbf{p}^i}{\|\Delta\mathbf{p}^i\|\,\|\mathbf{\Pi}\Delta\mathbf{p}^i\|} = \frac{\|\mathbf{\Pi}\Delta\mathbf{p}^i\|}{\|\Delta\mathbf{p}^i\|}, \tag{5}$$

which is related to a normal deviation of the coordinate curve from the tangent subspace. In any flat case, evidently, $\varphi^i = 0$ ($i = 1, \ldots, K$).

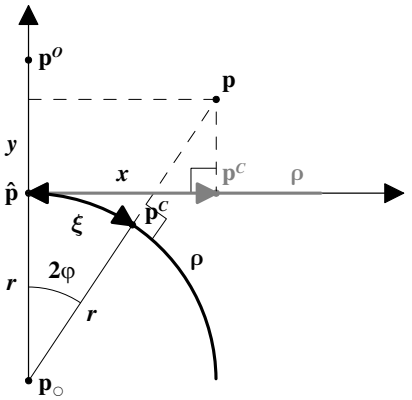

Fig. 2 Geometrical interpretation of a nonlinear LS-problem for $N = 2$ and $K = 1$. The grey and black thick lines are the estimation subspaces $\boldsymbol{\rho}$ in flat (straight) and nonflat (curved) cases respectively. The point $\mathbf{p}_\circ$ is the center of curvature of the curved estimation line and r is the radius of curvature; $\mathbf{p}$ is an arbitrary point in the observation plane with coordinates x and y; $\mathbf{p}^C$ (grey and black) are the orthogonal projections of the point $\mathbf{p}$ onto the estimation lines, i.e. they are also the LS-estimation points as if $\mathbf{p}$ would be a point of observations; their coordinates are x in the straight case and ξ in the nonstraight case; $\mathbf{p}^O$, $\hat{\mathbf{p}}$ and φ have the same meanings as in Fig. 1

Finally, using the angular values, we approximately find the normal curvatures

$$\kappa^i \approx \frac{2\varphi^i}{\|\Delta\mathbf{p}^i\|} \quad (i = 1, \ldots, K). \tag{6}$$

So we can consider the maximum of the normal curvatures

$$\kappa = \max_{i=1,\ldots,K} \kappa^i \tag{7}$$

as an index of intrinsic nonlinearity. However, we do not know at all yet how large its value must be for the intrinsic nonlinearity to be regarded as strong. What is its boundary value between the values of weak and strong intrinsic nonlinearity? By the way, the same question concerns the angular index (1). In the next section we make an evaluation of this boundary value.

3 Index of Intrinsic Nonlinearity

Consider a nonlinear but flat LS-problem with $N = 2$ and $K = 1$ (Fig. 2). The observation space of the problem is a plane with coordinates x and y while the estimation subspace $\boldsymbol{\rho}$ is a straight line on the plane. Suppose that the estimation line coincides with the x-axis perpendicular to the y-axis, the estimation $\hat{\mathbf{p}}$ being the center of the coordinate system.

Bend now the line as a flexible ruler fixed at $\hat{\mathbf{p}}$, laying it on a circle of radius r (centered at the point $\mathbf{p}_\circ$). So we get a new estimation subspace being a curved line of curvature $\kappa = 1/r$. Let an arbitrary point of the observation plane have the coordinates $\mathbf{p} = (x, y)^T$. Obviously, for this point the coordinate of the LS-estimation $\mathbf{p}^C$ on the straight estimation line is x and it differs from that on the curved estimation line ξ (Fig. 2). The question is how essential the difference between x and ξ is.

According to the geometry of the problem, a relative change of the LS-solution due to the curving of the estimation line is

$$\frac{\delta x}{x} = \frac{x-\xi}{x}, \quad \text{where} \quad \xi = r \arctan \frac{x}{y+r}.$$

Assume that $r \gg \|\mathbf{p} - \hat{\mathbf{p}}\|$ (therefore $r \gg |y|$) then up to first order small values we have

$$\frac{\delta x}{x} = \frac{y}{r}. \tag{8}$$

In the general case, the curving of the estimation subspace leads to similar relative change values $\|\delta\mathbf{p}^C\|/\|\mathbf{p}^C - \hat{\mathbf{p}}\|$. However, we should be interested only in the relative change along the coordinate curve with the maximum normal curvature κ. To that we can use (8):

$$\frac{\|\delta\mathbf{p}^C\|}{\|\mathbf{p}^C - \hat{\mathbf{p}}\|} = \left|\frac{\delta x}{x}\right| = \frac{|y|}{r} = \kappa|y|, \quad \text{where} \quad y = \frac{(\mathbf{p} - \hat{\mathbf{p}}) \cdot (\mathbf{p}^O - \hat{\mathbf{p}})}{\|\mathbf{p}^O - \hat{\mathbf{p}}\|}, \tag{9}$$

as if we would consider the effect of the curving in the x–y plane where the x-axis and y-axis are orientated along respectively the tangent to the curve at the point $\hat{\mathbf{p}}$ and the normal to the estimation subspace, i.e. along the direction to the point $\mathbf{p}^O$.

Further, any relative change value $\|\delta\mathbf{p}^C\|/\|\mathbf{p}^C - \hat{\mathbf{p}}\|$ in the estimation subspace inevitably cause a response value $\|\delta\mathbf{q}\|/\|\mathbf{q} - \hat{\mathbf{q}}\|$ in the parametric space. To establish linkage between them, we can use the linear relations

$$\delta\mathbf{p}^C = \mathbf{p}'_\mathbf{q}\delta\mathbf{q}, \quad \mathbf{p}^C - \hat{\mathbf{p}} = \mathbf{p}'_\mathbf{q}(\mathbf{q} - \hat{\mathbf{q}}).$$

They give the quadratic forms

$$\|\delta\mathbf{p}^C\|^2 = \delta\mathbf{q}^T(\mathbf{p}'_\mathbf{q})^T\mathbf{p}'_\mathbf{q}\delta\mathbf{q}, \quad \|\mathbf{p}^C - \hat{\mathbf{p}}\|^2 = (\mathbf{q} - \hat{\mathbf{q}})^T(\mathbf{p}'_\mathbf{q})^T\mathbf{p}'_\mathbf{q}(\mathbf{q} - \hat{\mathbf{q}})$$

with respect to $\delta\mathbf{q}$ and $\mathbf{q} - \hat{\mathbf{q}}$. Hence,

$$\|\delta\mathbf{q}\|^2_{\max} = \frac{\|\delta\mathbf{p}^C\|^2}{\lambda_{\min}}, \quad \|\mathbf{q} - \hat{\mathbf{q}}\|^2_{\min} = \frac{\|\mathbf{p}^C - \hat{\mathbf{p}}\|^2}{\lambda_{\max}},$$

where $\lambda_{\min}$ and $\lambda_{\max}$ are respectively the minimum and maximum eigenvalues of the normal matrix

$$\mathbf{Q} = (\mathbf{p}'_\mathbf{q})^T\mathbf{p}'_\mathbf{q}. \tag{10}$$

So we obtain the maximum of all possible relative change values in the parametric space:

$$\frac{\|\delta\mathbf{q}\|_{\max}}{\|\mathbf{q} - \hat{\mathbf{q}}\|_{\min}} = c\frac{\|\delta\mathbf{p}^C\|}{\|\mathbf{p}^C - \hat{\mathbf{p}}\|}, \quad \text{where} \quad c^2 = \operatorname{cond}\mathbf{Q} = \frac{\lambda_{\max}}{\lambda_{\min}}. \tag{11}$$

Let $f(\mathbf{q})$ be a probability density function in the parametric space $\mathbf{q}$. Suppose that the curving of the estimation subspace results in the parametric transformation $\gamma\mathbf{q}$, where $\gamma = 1 \pm \|\delta\mathbf{q}\|_{\max}/\|\mathbf{q} - \hat{\mathbf{q}}\|_{\min}$. This causes the change of the probability density function

$$g(\gamma\mathbf{q}) = g(\mathbf{\Gamma}\mathbf{q}) = \det\mathbf{\Gamma}^{-1} f(\mathbf{q}) = f(\mathbf{q})/\gamma^K, \quad \mathbf{\Gamma} = \operatorname{diag}(\gamma, \ldots, \gamma),$$

and, consequently, the relative deviation of the probability mass P inside any small region

$$\frac{|\delta P|}{P} \approx \frac{|g - f|}{f} \approx |\gamma^{-K} - 1| \approx K\frac{\|\delta\mathbf{q}\|_{\max}}{\|\mathbf{q} - \hat{\mathbf{q}}\|_{\min}}.$$

According to (9), up to first order small values we have

$$\frac{|\delta P|}{P} = cK\kappa|y|.$$

Thus we can get the critical value κ^* that the curvature κ must not reach, i.e. the condition

$$\kappa < \kappa^* = \frac{|\delta P/P|_{\text{tol}}}{cK|y|_{\max}} \quad \text{or} \quad \varkappa = \frac{\kappa}{\kappa^*} < 1 \tag{12}$$

must hold. Here $|y|_{\max}$ is the maximum of possible values $|y|$ and $|\delta P/P|_{\text{tol}}$ is a tolerable relative probability error. The dimensionless quantity $\varkappa$ in (12) is just that we propose to take as an index of intrinsic nonlinearity instead of κ: if $\varkappa < 1$ then the intrinsic nonlinearity is weak, else it is strong.

In practice, having solved an inverse problem, we have already most of the values to calculate the index $\varkappa$. These are the derivative matrix $\mathbf{p}'_{\mathbf{q}}$ (for $\mathbf{\Pi}$ and $\mathbf{Q}$), the condition number c (11) as well as the number of model parameters K and the tolerable relative probability error $|\delta P/P|_{\text{tol}}$ known before solving the problem. The value $|y|_{\max}$ stands as a maximum possible value of observation error. We can specify it under some priori considerations although we can also take the root-mean-square error of the processed observations, which is known after solving the problem too, or a multiple of it with small integer multipliers, say, not greater than 5. We have but to find variations (3) using the model to calculate κ (7) and then $\varkappa$ (12).

It is worth noting that the condition number c (12) directly depends on the model parameters $\mathbf{q}$ and so one should speak about weak or strong intrinsic nonlinearity only in terms of these parameters. Accordingly any reparametrization is able either to weaken or to aggravate the intrinsic nonlinearity while the normal curvature κ remains the same.

In fact the index $\varkappa$ (7) should be regarded as a measure of the contribution of intrinsic nonlinearity to the discrepancy between probabilistic estimates within the original nonlinear model $\mathbf{p}^C = \mathbf{p}^C(\mathbf{q})$ and its linearization. For example, if we use a covariance matrix for investigating parametric uncertainty then the index enables us to see how inaccurate our probabilistic estimations within a linearized model can be due to the intrinsic nonlinearity. It stands to reason that a large value of the index signals on strong intrinsic nonlinearity. Though we can still obtain quite acceptable probabilistic estimations if we resort to the method of disturbed observations. The question on its efficiency in strongly intrinsically nonlinear problems is discussed in the next section.

4 Method of Disturbed Observations

Further, we briefly remind the reader of the essence of the technique we call the method of disturbed observations and also discuss its capability allowing to simulate uncertainty clouds eligible even in strongly intrinsically nonlinear problems. In more detail the method is expounded in (Avdyushev, 2011).

Let $\boldsymbol{\nu}_J$ be a J-dimensional standard normal random vector: $\boldsymbol{\nu}_J \sim \mathcal{N}(\mathbf{0}, \mathbf{I}_{J\times J})$, where $\dim \mathbf{0} = J$ and $\mathbf{I}_{J\times J}$ is the $J\times J$ identity matrix. Observation errors are supposed to be normal variates with zero mean and an observational error variance σ^2, then $\delta\mathbf{p}^O = \sigma\boldsymbol{\nu}_N$. Therefore, in any flat case $\hat{\mathbf{p}} - \bar{\mathbf{p}} = \sigma\boldsymbol{\nu}_K$ as this vector difference is a projection of $\delta\mathbf{p}^O = \mathbf{p}^O - \bar{\mathbf{p}}$ onto the K-dimensional estimation subspace $\boldsymbol{\rho}$. Thus, though the point $\bar{\mathbf{p}}$ corresponding to the true orbital parameter values $\bar{\mathbf{q}}$ is nonrandom, its deviation from the estimation $\hat{\mathbf{p}}$ is random and normal, just the same as the deviation of $\hat{\mathbf{p}}$ from $\bar{\mathbf{p}}$. Consequently, if we get some estimation $\hat{\mathbf{p}}$ from a sample of observations $\mathbf{p}^O$ then we can expect the location of the

point $\bar{\mathbf{p}}$ (corresponding to the exact observations) in compliance with the normal distribution $\mathcal{N}(\hat{\mathbf{p}}, \sigma^2\mathbf{I}_{K\times K})$. In other words, the probability distribution of the unknown point $\bar{\mathbf{p}}$ relative to the estimation $\hat{\mathbf{p}}$ obtained from the sample of observations $\mathbf{p}^O$ must be the same as that of $\hat{\mathbf{p}}$ obtained from all possible samples of observations $\mathbf{p}^O = \bar{\mathbf{p}} + \sigma\boldsymbol{\nu}_N$ relative to $\bar{\mathbf{p}}$.

According to LS-theory the estimation $\hat{\mathbf{p}}$ is the point $\mathbf{p}^C$ of the estimation subspace $\boldsymbol{\rho}$ that gives the minimum squared distance S to the point of observations $\mathbf{p}^O$ (Fig. 1):

$$\hat{\mathbf{p}} \in \boldsymbol{\rho} : S = \|\mathbf{p}^O - \mathbf{p}^C\|^2 = \|\bar{\mathbf{p}} + \delta\mathbf{p}^O - \mathbf{p}^C\|^2 \to \min. \tag{13}$$

Since the vector of observation errors $\delta\mathbf{p}^O$ is random, the estimation $\hat{\mathbf{p}}$ is random as well:

$$\delta\mathbf{p}^O = \sigma\boldsymbol{\nu}_N \sim \mathcal{N}(\mathbf{0}, \sigma^2\mathbf{I}_{N\times N}) \quad \text{and} \quad \hat{\mathbf{p}} = \bar{\mathbf{p}} + \sigma\boldsymbol{\nu}_K \sim \mathcal{N}(\bar{\mathbf{p}}, \sigma^2\mathbf{I}_{K\times K}).$$

Hence it gets evident that for simulating the probability distribution of the unknown point $\bar{\mathbf{p}}$ we can use (13) substituting the known estimation $\hat{\mathbf{p}}$ for $\bar{\mathbf{p}}$. So, repeatedly generating the normal random vector $\delta\mathbf{p}^O = \sigma\boldsymbol{\nu}_N$ and solving the LS-problem (13) with $\hat{\mathbf{p}}$ instead of $\bar{\mathbf{p}}$:

$$\mathbf{p} \in \boldsymbol{\rho} : \|\hat{\mathbf{p}} + \sigma\boldsymbol{\nu}_N - \mathbf{p}^C\|^2 \to \min, \tag{14}$$

we can numerically simulate a cloud in the estimation subspace which discretely describes the probability distribution of $\bar{\mathbf{p}}$, i.e. $\bar{\mathbf{p}} \sim \mathcal{N}(\hat{\mathbf{p}}, \sigma^2\mathbf{I}_{K\times K})$. To simulate a similar cloud of uncertainty in the parametric space $\mathbf{q}$ we have to solve repeatedly the same LS-problem but relative to the model parameters:

$$\mathbf{q} : \|\hat{\mathbf{p}} + \sigma\boldsymbol{\nu}_N - \mathbf{p}^C(\mathbf{q})\|^2 \to \min. \tag{15}$$

In a linear case, it gives a set of virtual dynamic states $\mathbf{q}$ corresponding to the normal distribution $\mathcal{N}(\hat{\mathbf{q}}, \sigma^2\mathbf{Q}^{-1}_{K\times K})$.

From a geometric point of view the technique (15) consists in projecting a cloud of uncertainty $\hat{\mathbf{p}} + \sigma\boldsymbol{\nu}_N$ in the observation space orthogonally onto the estimation subspace $\boldsymbol{\rho}$ and further mapping it into the parametric space $\mathbf{q}$ in conformity with the model $\mathbf{p}^C = \mathbf{p}^C(\mathbf{q})$. When the estimation subspace is flat, there is no difference to disturb whether the estimation $\hat{\mathbf{p}}$ or the point of observations $\mathbf{p}^O$. In practice it is convenient to add the disturbance $\sigma\boldsymbol{\nu}_N$ straight to the observations $\mathbf{p}^O$, this is why we call this technique the method of disturbed observations (Avdyushev, 2011).

If the error variance σ^2 is unknown (as so often is the case in practice) then instead of it one takes an unbiased estimate of the variance $\hat{\sigma}^2 = S(\hat{\mathbf{q}})/(N-K)$, which, as a statistics, is related to the chi-squared distribution with $N-K$ degrees of freedom:

$$\hat{\sigma}^2 = \sigma^2\frac{\chi^2_{N-K}}{N-K}, \tag{16}$$

since $S(\hat{\mathbf{q}}) = \|\mathbf{p}^O - \hat{\mathbf{p}}\|^2$, while the vector $\mathbf{p}^O - \hat{\mathbf{p}} = \sigma\boldsymbol{\nu}_{N-K}$ is normally distributed in the $(N-K)$-dimensional subspace orthogonal to the estimation subspace. After substituting $\hat{\sigma}$ for σ, the method (15) requires modifying by introducing a modulating random factor μ (Avdyushev, 2011):

$$\mathbf{q} : \|\hat{\mathbf{p}} + \mu\hat{\sigma}\boldsymbol{\nu}_N - \mathbf{p}^C(\mathbf{q})\|^2 \to \min, \quad \mu = \sqrt{(N-K)/\chi^2_{N-K}}. \tag{17}$$

If the inverse problem is linear then, unlike (15), the modification (17) gives a set of virtual dynamic states $\mathbf{q}$ which corresponds Hotelling's distribution (Anderson, 1958) being a

generalization of Student's distribution to multidimensional cases. Obviously, $\mu \to 1$ and $\hat{\sigma}^2 \to \sigma^2$ as $N \to \infty$, therefore, when N is very large one can take $\mu = 1$.

Imagine now that the estimation subspace has a constant normal curvature and the error variance σ^2 is known. What is interesting is that however large the curvature is, the method of disturbed observations (15) turns out still good for simulating a cloud of uncertainty while the inverse problem can be strongly intrinsically nonlinear. In fact, for any point of the estimation subspace (including either $\bar{\mathbf{p}}$ or $\hat{\mathbf{p}}$) which we disturb, the distribution of its disturbances projected onto the subspace is always the same. Consequently, according to (14) the simulated distribution of the unknown point $\bar{\mathbf{p}}$ relative to $\hat{\mathbf{p}}$ will exactly reproduce the distribution of the estimation $\hat{\mathbf{p}}$ obtained from all possible observations $\mathbf{p}^O = \bar{\mathbf{p}} + \sigma\boldsymbol{\nu}_N$ relative to $\bar{\mathbf{p}}$. It is just the same as in a flat case. This is easily seen by referring to a simple problem with $N = 3$ and $K = 2$ (see Fig. 1) (or $K = 1$), where the estimation subspace is a spherical surface (or a circular arc).

When the error variance σ^2 is unknown and the normal curvature is large and variable, there is no strict ground to use the technique (17) since the simulated distribution of $\bar{\mathbf{p}}$ relative to $\hat{\mathbf{p}}$ will not represent the distribution of $\hat{\mathbf{p}}$ relative to $\bar{\mathbf{p}}$ as above and the distribution of $\hat{\sigma}^2$ will not correspond rigorously to (16). Nevertheless, as our numerical results show in the next section, the normal curvature (or local nonflatness) in inverse problems of celestial mechanics is so insignificant that it practically must not affect the distribution of the virtual dynamic states simulated by the method of disturbed observations.

5 Numerical Results

5.1 Test Asteroid Problems

The main aim of our investigations was to find out how strong the intrinsic nonlinearity can be in inverse problems of celestial mechanics, i.e. when the orbit of a celestial body is determined from its astrometric observations. The question of nonlinearity is generally the most significant in studying the orbital dynamics of potentially hazardous asteroids when the probability that an asteroid will collide with the Earth requires estimating by stochastic simulation. Therefore we set our numerical experiment so that its results would be related to the asteroid problems.

Preliminary investigation had shown us (Avdyushev, 2011) that the intrinsic nonlinearity got stronger as the observed orbital arc shortened. So we focused our attention on the inverse problems with very short observed orbital arcs, and to come to some general conclusions, we used simulated observations (without errors) rather than real ones, more by token, the intrinsic nonlinearity is rather a property of an orbital model we accept than that of real observations the model represents.

Since any short orbital arc is well described by a Keplerian orbit, we made all our calculations within the two-body theory. First we simulated asteroid positions in heliocentric coordinates $\mathbf{x}$ on some Keplerian orbit (with the unit semi-major axis) at uniformly distributed times (Fig. 3), then projected the positions onto the celestial sphere centered at an observation point (or a position of the observer, viz., we mean the Earth) $\mathbf{x}^O$ moving in a circular orbit, and thereby obtained the (geocentric) angle observations — the right ascensions α and the declinations δ.

For every combination of the simulated orbital positions, we obtained 10^6 various samples of angle observations by varying an initial position of the observation point $\mathbf{x}_0^O$. For an

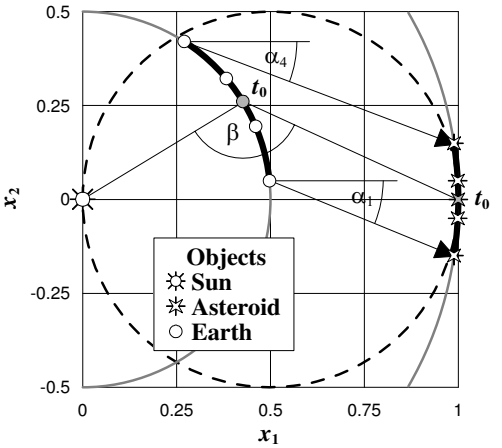

Fig. 3 Simulation of observations (x_1–x_2 plane projection). Here the symbols indicate the positions of the celestial bodies at different times: the white ones are at times of observations and the grey ones are at an initial time t_0; α_1 and α_4 are the right ascensions (observations) at the first and last (fourth) times; the thick black lines are the trajectories of Earth and asteroid motions in orbits (the grey lines) over the observation period. In the figure is shown a particular case when the asteroid and the observation point (Earth) move in circular orbits of radiuses 1 and 0.5 respectively in the same plane x_1–x_2, i.e. $x_3 = 0$ and $\delta = 0$. Though in the general case the orbital plane of the observation point differs from that of the asteroid and depends on an initial position of the observation point which is chosen at random inside the tolerance sphere (the dashed circle is its boundary) to satisfy the observability condition $\beta > 90°$.

asteroid to be observable in the night sky we supposed that the angle β between the directions from the observation point to the Sun and the asteroid should be greater than 90°. Thus we varied the initial position of the observation point $\mathbf{x}_0^O$ randomly and uniformly inside the sphere for that the Sun (the coordinate origin) and the initial asteroid position $\mathbf{x}_0$ were diametrically opposite points (Fig. 3), and for every sample of angle observations we checked if inequality (12) held.

We had to create extremely bad conditions for the inverse problems. Therefore, we simulated only four pairs of angle observations without errors $\mathbf{p}^O = \mathbf{p}^C = (\alpha_1, \delta_1, \ldots, \alpha_4, \delta_4)^T$ on very short observed orbital arcs up to $2\pi \cdot 10^{-3}$ long (e.g. for Ceres it is about 2 days). The dynamic state vector $\mathbf{q} = (\mathbf{x}_0, \dot{\mathbf{x}}_0)^T$, the position and velocity related to some initial time t_0 within the observation span, was considered as determined from the observations $\mathbf{p}^O$. Accordingly, $K = 6$ and $N = 8$. For simulating the motion of the observation point $\mathbf{x}^O$ its initial position $\mathbf{x}_0^O$ was selected randomly while its initial velocity $\dot{\mathbf{x}}_0^O$ was specified so that it was circular and perpendicular to the applicate axis.

For potentially hazardous asteroids the best accuracy of CCD observations in 2016 is about $\sigma = 0.2''$ (www.minorplanetcenter.net). Taking into account the three sigma rule, in (12) we specified $|y|_{\max} = 3 \cdot 10^{-6} \approx 3\sigma = 0.6''$. Since in practice usually only the first digit for a value of the probability P is of interest, we took $|\delta P/P|_{\text{tol}} = 5 \cdot 10^{-2}$.

To evaluate the normal curvature κ (7) for inequality (12), analytic formulae for the partial derivatives $\mathbf{p}'_{\mathbf{q}}$ were required. They were obtained by directly differentiating the formulae of the two-body theory and then converting to the space of the angle observations. For every parameter variation $\Delta\zeta_i$ (3) the square root of the diagonal element c_{ii} of the covariance matrix $\mathbf{C} = \sigma^2\mathbf{Q}^{-1}$ was taken: it just provided the best calculating accuracy for κ.

Now, after the general description of the experiment, the basic consecutive stages in its implementation are worth marking out.

1. At first we specified orbital elements and converted them into the orbital parameters $\mathbf{q} = (\mathbf{x}_0, \dot{\mathbf{x}}_0)^T$ at the time $t_0 = 0$.
2. Simulated four positions on the Keplerian orbit at the times $t_1, \ldots, t_4$: $-t_1 = -3t_2 = 3t_3 = t_4 = \Delta t/2$, where the observation span $\Delta t = t_4 - t_1$ corresponded to a given observed orbital arc.
3. Set an initial position of the observation point $\mathbf{x}_0^O$ at random inside the sphere determined by the observability condition $\beta > 90^\circ$ and simulated four observation points $\mathbf{x}^O$ on the circular orbit passing the point $\mathbf{x}_0^O$ at the same times as above.
4. Obtained the angular positions $\mathbf{p}^C = (\alpha_1, \delta_1, \ldots, \alpha_4, \delta_4)^T$.
5. Calculated the partial derivatives $\mathbf{p}'_\mathbf{q}$, the idempotent matrix $\mathbf{\Pi}$ (4), the normal matrix $\mathbf{Q}$ (10), and also the condition number c (11).
6. Varying sequentially every component of $\mathbf{q}$ by the corresponding value $\Delta\zeta$ and repeating stages 2 and 4, we found six variations in the angular positions $\Delta\mathbf{p}$ (3).
7. Finally, according to (5)–(7) and (12), we calculated φ^i and κ^i ($i = 1, \ldots, 6$) as well as κ and $\varkappa$.

For every orbit the sequence of stages 3–7 was repeated 10^6 times at different random initial positions of the observation point $\mathbf{x}_0^O$.

We examined inverse problems for orbits of all kinds. There were various distributions of the intial observation points for that the inverse problems became strongly intrinsically nonlinear, i.e. when $\varkappa > 1$. As examples, in Fig. 4–6 distributions like those are shown for three orbits — I, II, and III — determined from observations on three observed orbital arcs s long — $s/2\pi = 10^{-1}, 10^{-2}$, and 10^{-3}. All the orbits have the unit semi-major axes ($a = 1$) while their inclinations I and arguments of pericenters ω are zero. The other orbital elements — the eccentricities e, longitudes of ascending nodes Ω, and mean anomalies M_0 at t_0 — are in the captions to the figures. The amounts of the inverse problems with $\varkappa > 1$ percentage-wise for every pair orbit–arc are given in Table 1 (Strongly intrinsically nonlinear problems). Here are also presented both the minimum and maximum orders of condition numbers (Conditionality) and the maxima of the value that indicates how the estimation subspace differs from a flat one in the neighborhood of the LS-estimation (Local nonflatness).

So the figures and also the percentage of strongly intrinsically nonlinear problems in Table 1 evince that the intrinsic nonlinearity can be strong enough to appreciably affect probabilistic estimates, especially at the extra short observed orbital arcs. Nevertheless there are configurations Sun–Earth-asteroid when the intrinsic nonlinearity is very weak, and some of them (Fig. 6) correspond to the favorable circumstances for discovery of new asteroids, viz., when the observed objects are in oppositions.

In actuality, the strong intrinsic nonlinearity is mainly caused by very large condition numbers c (see their orders in Table 1). Only for orbit III, when $c \leq 10^4$, there is revealed no strongly intrinsically nonlinear problem. Therefore we suppose that if $c > 10^4$ then it already gives cause for us to suspect that we deal with strong intrinsic nonlinearity.

Generally the condition number c (11) indicates how sensitive the estimation $\hat{\mathbf{q}}$ in the parametric space to variations of the estimation $\hat{\mathbf{p}}$ in the observation space can be. We are certainly interested in the variations like (9) due to the normal curvature of the estimation subspace. It is remarkable that in our inverse problems they relative to the radius r of the normal curvature κ turn out small enough. We judge it by the ratio $|y|_{\max}/r = 3\sigma\kappa$ which can be regarded as an index of local nonflatness of the estimation subspace inside the cloud of disturbances $\hat{\mathbf{p}} + \sigma\boldsymbol{\nu}_N$.

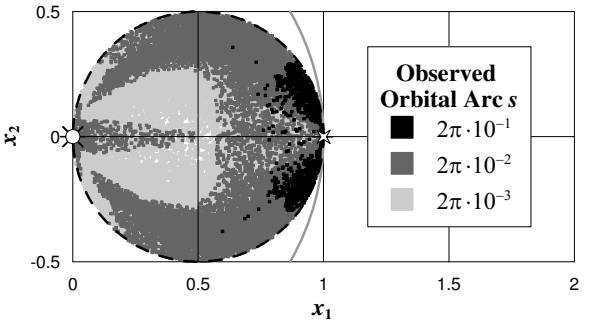

Fig. 4 Distributions of the intial positions of the observation point $\mathbf{x}_0^O$ for that $\varkappa > 1$. Orbit I: $e = 0$; $\Omega = 0$; $M_0 = 0$

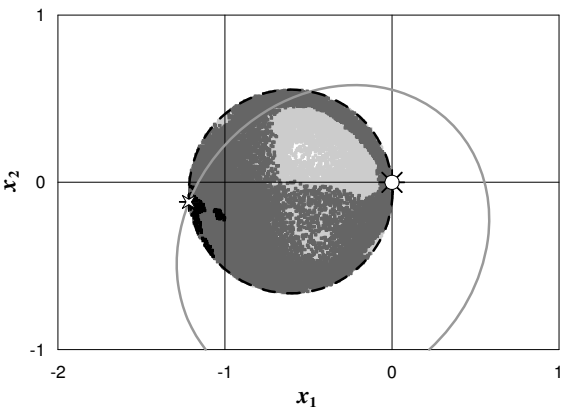

Fig. 5 The same as in Fig. 4 but for orbit II: $e = 0.5$; $\Omega = 45°$; $M_0 = 90°$

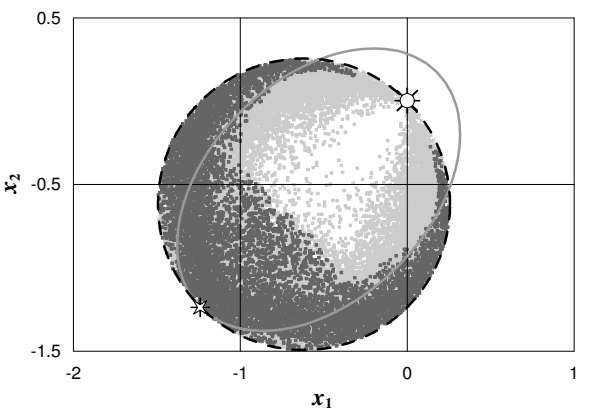

Fig. 6 The same as in Fig. 4 but for orbit III: $e = 0.75$; $\Omega = 45°$; $M_0 = 180°$

Table 1 Numerical results. Test asteroid orbits

Observed orbital arc	Strongly intrinsically nonlinear problems (%)			Conditionality $\lg c_{\min}$–$\lg c_{\max}$			Local nonflatness $3\sigma\kappa_{\max}$		
$s/2\pi$	I	II	III	I	II	III	I	II	III
10^{-1}	2	1	0	1–5	1–5	1–4	$2 \cdot 10^{-5}$	10^{-4}	$5 \cdot 10^{-5}$
10^{-2}	30	35	17	3–8	3–8	3–7	10^{-4}	10^{-4}	10^{-4}
10^{-3}	75	80	53	5–11	5–10	4–10	10^{-4}	$3 \cdot 10^{-4}$	$2 \cdot 10^{-4}$

Table 2 Orbital elements of real asteroids

Asteroid	a (AU)	T (days)	e	I (°)	Ω (°)	ω (°)	v_0 (°)
2016 PZ39	2.35	1315	0.80	4.3	79.7	118.3	118.7
2016 PQ39	1.68	798	0.54	7.9	18.4	53.7	248.8
2016 PO39	1.83	901	0.51	31.6	336.3	219.3	128.8

For orbits I, II and III the quantity $3\sigma\kappa$ did not exceed $3 \cdot 10^{-4}$ (Table 1). As for other test orbits with various orbital parameters, the maximum values of the quantity were of the same order. Compare, the horizon distance for a ground observer 4.7 km to the Earth's radius $6.4 \cdot 10^3$ km is about $7 \cdot 10^{-4}$. Meanwhile, Earth ellipsoid's surface within the horizon is seen as quite flat. Thus, in practice the local nonflatness of the estimation subspace is very small and therefore we can surely use the technique (17) for simulating and studying orbital uncertainty.

It should be noted that generally a small local nonflatness of the estimation subspace means as well that there exist such parameters relative to which the inverse problem could be weakly nonlinear and, moreover, with a very small condition number. How can we specify these parameters practically? That is a question of another paper. Anyway, Fig. 4–6 actually reveal the situations not only when the intrinsic nonlinearity is strong but when the components of the vectors $\mathbf{x}_0$ and $\dot{\mathbf{x}}_0$ as parameters are not so appropriate in terms of orbit determination.

5.2 Real Asteroid Problems

We also tried the index $\varkappa$ out to estimate the influence of intrinsic nonlinearity for some recently discovered and potentially hazardous asteroids — 2016 PZ39, 2016 PQ39, and 2016 PO39 (www.minorplanetcenter.net). Their orbital elements are given in Table 2, where T is the orbital period; v_0 is the true anomaly at t_0 (Table 3) and the inclination I is relative to the ecliptic. The asteroids were discovered in August 2016 and observed only for several nights (Table 3 and Fig. 7).

For processing the asteroid observations (www.minorplanetcenter.net) we used our own software package. Its nucleus is a numerical orbital model based on second-order differential equations in rectangular heliocentric coordinates describing an asteroid motion under the influence of gravitational forces of the Sun, the planets and the Moon. The equations are integrated numerically by Everhart's twelfth-order method (an implicit collocation Runge-Kutta method on Gauss-Lobatto spacing) (Avdyushev, 2010). So the orbital model provided asteroid positions accurate to 10^{-12} AU (10^{-6} arcsec), quite enough to process the observations. From the observations we determined the initial dynamic state vector $\mathbf{q} = (\mathbf{x}_0, \dot{\mathbf{x}}_0)^T$.

Since the observations represent short orbital arcs (see s in Table 4), they are little informative on orbital motion and, therefore, the asteroid orbits are determined unreliably: we can judge it by large values $\sigma_{\mathbf{x}} = \sqrt{c_{11} + c_{22} + c_{33}}$ and $\sigma_{\dot{\mathbf{x}}} = \sqrt{c_{44} + c_{55} + c_{66}}$ characterizing

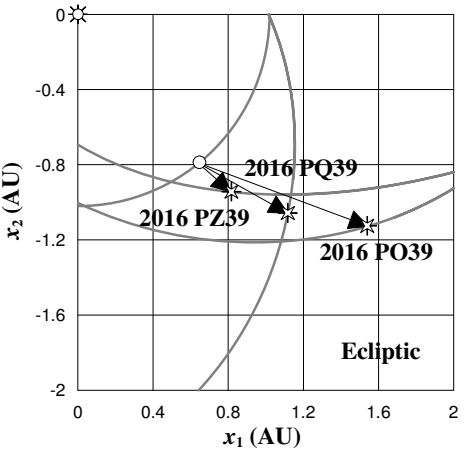

Fig. 7 Asteroid positions during observation

Table 3 Characteristics of inverse problems

Asteroid	N	Observation period	t_0	$\hat{\sigma}$ ($''$)	lg c	$\sigma_{\mathbf{x}}$ (AU)	$\sigma_{\dot{\mathbf{x}}}$ (AU/day)
2016 PZ39	76	10–13.08.2016	12.08.2016	0.20	4	10^{-3}	$4 \cdot 10^{-5}$
2016 PQ39	34	09–12.08.2016	11.08.2016	0.16	5	$2 \cdot 10^{-3}$	$4 \cdot 10^{-5}$
2016 PO39	28	07–12.08.2016	10.08.2016	0.32	5	$3 \cdot 10^{-2}$	$3 \cdot 10^{-4}$

Table 4 Numerical results. Real asteroid orbits

Asteroid	s (AU)	$\varkappa^{\dagger}$	$\varkappa$	$3\hat{\sigma}\kappa$
2016 PZ39	$5 \cdot 10^{-2}$	0.6	1.1	$6 \cdot 10^{-7}$
2016 PQ39	$4 \cdot 10^{-2}$	1.7	1.2	$3 \cdot 10^{-7}$
2016 PO39	$6 \cdot 10^{-2}$	4.3	14.0	$9 \cdot 10^{-7}$

initial position and velocity uncertainties (Table 3). Here c_{ii} ($i = 1, \ldots, 6$) are the diagonal elements of the covariance matrix $\mathbf{C} = \hat{\sigma}^2\mathbf{Q}^{-1}$, the variances of the parameters $\mathbf{q}$; $\hat{\sigma}$ is the root-mean-square error of the processed observations. Compare with the values $\sigma_{\mathbf{x}} = 2 \cdot 10^{-8}$ AU and $\sigma_{\dot{\mathbf{x}}} = 4 \cdot 10^{-10}$ AU/day for Apophis whose orbit is well determined from a lot of observations ($N > 8000$) over a span more than ten years.

Sizeable orbital uncertainty is usually associated with a strong influence of both total and intrinsic nonlinearities. Indeed, the indices of intrinsic nonlinearity $\varkappa$ are greater than the unit (Table 4) as well as those of total nonlinearity $\varkappa^{\dagger}$ considerably exceed the critical value 0.1 (Avdyushev, 2011). By the way, for Apophis $\varkappa^{\dagger} = 2 \cdot 10^{-4}$.

It is worth reminding that the total nonlinearity contains both the parameter-effect and intrinsic nonlinearities (Bates and Watts, 1988). The former usually dominates and for this reason it is impossible to evaluate the intrinsic nonlinearity by the index $\varkappa^{\dagger}$. That $\varkappa^{\dagger}$ relating to the general is less than $\varkappa$ relating to the particular (for 2016 PZ39 and 2016 PO39) should not cause perplexity since they in nature are different values.

The large indices $\varkappa^{\dagger}$ mean that the clouds of uncertainty for all the three asteroids markedly differ from ellipsoidal ones as in linear problems and, therefore, any linear stochastic method here is not available. Meanwhile, the value $3\hat{\sigma}\kappa$ does not reach 10^{-6}, i.e. the local

nonflatness is very slight. Consequently the method of disturbed observations can be confidently used to simulate and investigate the uncertainties in the asteroid orbits.

The conditions of the inverse problems in this subsection are similar and if one compares them with those in the previous subsection then, considering the types of the asterod orbits and the circumstances of the observations, one can find that they are also similar to some conditions for orbit III at $s = 2\pi \cdot 10^{-2}$ (Fig. 6) when the observation points (Earth) relative to the Sun and asteroid are like in Fig. 7. Approximately, of the point set in Fig. 6, these must be the boundary observation points between the Sun and asteroid being in opposition.

6 Conclusion

So in the paper we introduced the index of intrinsic nonlinearity that allowed us to reveal the conditions of inverse problems of asteroid dynamics when the intrinsic nonlinearity get strong enough to appreciably affect probabilistic estimates. Having emploied the index in test inverse asteroid problems, we found out that mostly strong intrinsic nonlinearity occurs at the very short observed orbital arcs that the asteroids travel on for about a hundredth of their orbital periods and less.

The source of intrinsic nonlinearity is the local nonflatness of the estimation subspace specified a dynamical model in the observation space. According to our numerical results, the estimation subspace is virtually almost locally flat. However, in the parametric space the effect of intrinsic nonlinearity is exaggerated mainly by the ill-conditioning of the inverse problem. As we ascertained, a condition number $c > 10^4$ indicates that we deal with strong intrinsic nonlinearity. Nevertheless, a reparametrization can considerably make better the conditionality and, as we suppose, the choice of the most appropriate parameters in terms of orbit determination will be a topic of our further investigations.

We also discussed a question about the practical ground of the method of disturbed observations to stochastically simulate orbital uncertainty under the condition of strong intrinsic nonlinearity. From a geometric point of view, the efficiency of the method directly depends only on the local nonflatness of the estimation subspace that, as our results showed, is negligible in practice. Therefore, even if the nonlinearity in the parametric space is extremely strong, the method is quite acceptable to adequately describe the orbital uncertainty.

Strong nonlinearity typically occurs when determining the orbit of a recently discovered celestial body from a small sample of observations over a very short observed orbital arc. Lots of new space objects are discovered now and undoubtedly the method of disturbed observations could become a reliable tool for researching their orbital uncertainties.

References

Anderson, T.W.: An Introduction to Multivariate Statistical Analysis. John Wiley & Sons Inc. (1958)

Avdyushev, V.A.: A New Method for the Statistical Simulation of the Virtual Values of Parameters in Inverse Orbital Dynamics Problems // Sol. Syst. Res. 43, 6, 543–551 (2009)

Avdyushev, V.A.: Numerical Orbit Simulation. Tomsk: STL (2010) (in Russian)

Avdyushev, V.A.: Nonlinear Methods of Statistic Simulation of Virtual Parameter Values for Investigating Uncertainties in Orbits Determined from Observations. Celest. Mech. 110 (4), 369–388 (2011)

Avdyushev, V.A., Banschikova, M.A.: Regions of Possible Motions for New Jovian Satellites. Sol. Syst. Res. 41, 5, 413–419 (2007)

Bates, D.M., Watts, D.G.: Nonlinear Regression Analysis and Its Applications. John Wiley and Sons Ltd. New York–Chichester–Brisbane–Toronto–Singapore (1988)

Beale, E.M.L.: Confidence Regions in Non-Linear Estimation. J. R. Statist. Soc. 22, 1, 41–88 (1960)

Bordovitsyna, T., Avdyushev, V., Chernitsov, A.: New Trends in Numerical Simulation of the Motion of Small Bodies of the Solar System. Celest. Mech. 80, 3, 227–247 (2001)

Chernitsov, A.M., Baturin, A.P., Tamarov, V.A.: Analysis of Some Methods for Determination of Probabilistic Evolution of Motion of Solar System's Small Bodies. Solar System Research. 32, 405–413 (1998)

Desmars, J., Arlot, S., Arlot, J.-E., Lainey, V., Vienne, A.: Estimating the Accuracy of Satellite Ephemerides Using the Bootstrap Method. A&A. 62, 321–330 (2009)

Draper, N.R., Smith, H.: Applied Regression Analysis. John Wiley and Sons Ltd. New York–Chichester–Brisbane–Toronto–Singapore (1981)

Emel'yanov, N.: Precision of the Ephemerides of Outer Planetary Satellites. PSS. 58, 3, 411–420 (2010)

Milani, A., Gronchi, G.: Theory of Orbit Determination. Cambridge, UK: Cambridge University Press (2009)

Muinonen, K., Virtanen, J., Granvik, M., Laakso, T.: Asteroid Orbits Using Phase-Space Volumes of Variation. Mon. Not. R. Astron. Soc. 368, 809–818 (2006)

Press, W.H., Flannery, B.P., Teukolsky, S.A., Vetterling, W.T.: Numerical Recipes: The Art of Scientific Computing. Cambridge: University Press (1987)

Virtanen, J., Muinonen, K., Bowell, E.: Statistical Ranging of Asteroid Orbits. Icarus. 154, 412–431 (2001)

Williams, I.P., Ryabova, G.O., Baturin, A.P., Chernitsov, A.M.: Are asteroid 2003 EH1 and comet C/1490 Y1 dynamically related? Earth, Moon, and Planets. 95, 11–18 (2005)